arXiv:2107.06652v2 [cs.CV] 6 Aug 2021

Self-Supervised Multi-Modal Alignment For Whole Body Medical Imaging

Rhydian Windsor[1], Amir Jamaludin[1], Timor Kadir[1,2], and Andrew Zisserman[1]

[1] Visual Geometry Group, Department of Engineering Science, University of Oxford, Oxford, UK
[2] Plexalis Ltd., Thame, UK
rhydian@robots.ox.ac.uk

Abstract. This paper explores the use of self-supervised deep learning in medical imaging in cases where two scan modalities are available for the same subject. Specifically, we use a large publicly-available dataset of over 20,000 subjects from the UK Biobank with both whole body Dixon technique magnetic resonance (MR) scans and also dual-energy x-ray absorptiometry (DXA) scans. We make three contributions: (i) We introduce a multi-modal image-matching contrastive framework, that is able to learn to match different-modality scans of the same subject with high accuracy. (ii) Without any adaption, we show that the correspondences learnt during this contrastive training step can be used to perform automatic cross-modal scan registration in a completely unsupervised manner. (iii) Finally, we use these registrations to transfer segmentation maps from the DXA scans to the MR scans where they are used to train a network to segment anatomical regions without requiring ground-truth MR examples. To aid further research, our code will be made publicly available[†].

1 Introduction

A common difficulty in using deep learning for medical tasks is acquiring high-quality annotated datasets. There are several reasons for this: (1) using patient data requires ethical clearance, anonymisation and careful curation; (2) generating ground-truth labels may require expertise from clinicians whose time is limited and expensive; (3) clinical datasets are typically highly class-imbalanced with vastly more negative than positive examples. Thus acquiring sufficiently large datasets is often expensive, time-consuming, and frequently infeasible.

As such, there is great interest in developing machine learning methods to use medical data and annotations efficiently. Examples of successful previous approaches include aggressive data augmentation [29] and generating synthetic images for training [10]. Alternatively, one can use *self-supervised pre-training* to learn useful representations of data, reducing annotation requirements for downstream learning tasks. This method has already shown much success in

[†] https://github.com/rwindsor1/biobank-self-supervised-alignment

other areas of machine learning such as natural image classification [8, 14, 16] and natural language processing [6, 9, 25, 28].

In this paper, we develop a self-supervised learning approach for cases where pairs of different-modality images corresponding to the same subject are available. We introduce a novel pre-training task, where a model must to match together different-modality scans showing the same subject by comparing them in a joint, modality-invariant embedding space. If these modalities are substantially different in appearance, the network must learn semantic data representations to solve this problem.

In itself, this is an important task. Embeddings obtained from the trained networks allow us to check if two different scans show the same subject in large anonymised datasets (by verifying that their embeddings match). It also defines a notion of similarity between scans that has applications in population studies. However, the main reward of our method are the semantic *spatial* representations of the data learnt during training which can be leveraged for a range of downstream tasks. In this paper we demonstrate the embeddings can be used for unsupervised rigid multi-modal scan registration, and cross-modal segmentation with opposite-modality annotations.

The layout of this paper is as follows: Section 2 describes the cross-modal matching task in detail, including the network architecture, loss function, and implementation details, as well as experimental results from a large, publically-available whole body scan dataset. Section 3 introduces algorithms using the embeddings learnt in Section 2 for fast unsupervised multi-modal scan registration which are shown to succeed in cases where conventional registration approaches fail. In Section 3.1, we then use these registrations to transfer segmentation maps between modalites, showing that by using the proposed cross-modal registration technique, anatomical annotations in DXAs can be used to train a segmentation network in MR scans.

1.1 Related Work

Self-supervised representation-learning is an incredibly active area of research at the moment. The current dominant praxis is to train models to perform challenging self-supervised learning tasks on a large dataset, and then fine-tune learnt representations for specific 'downstream' tasks using smaller, annotated datasets. Major successes have been reported in image classification [4,7,8,11,16], video understanding [13,27] and NLP [17,25,28], with self-supervised approaches often matching or exceeding the performance of fully-supervised approaches.

Due to the existence of a few large, publically available datasets (such as [20]), yet lack of large annotated datasets suitable for most medical tasks, self-supervised learning shows great promise in the medical domain. For example, previous work has shown it can be used to improve automated diagnosis of intervertebral disc degeneration [19] and common segmentation tasks [33]. In [32], it also is shown that using multiple MR sequences in self-supervised learning improves performance in brain tumour segmentation.

Data with multiple modalities is a natural candidate for self-supervised approaches, as one can use information from one modality to predict information in the other. For example, previous work has shown self-supervised methods can benefit from fusion of the audio and visual streams available in natural video data [1, 2, 3, 21, 26]. In this paper we build on this multi-modal approach by extending it to explicit spatial registration across the modalities.

1.2 Dataset Information, Acquisition and Preparation

For the experiments in this paper we use data from the UK Biobank [31], a large corpus of open-access medical data taken from over 500,000 volunteer participants. A wide variety of data is available, including data related to imaging, genetics and health-related outcomes. In this study we focus on two whole body imaging modalities collected by the Biobank: (1) 1.5T, 6-minute dual-echo Dixon protocol magnetic resonance (MR) scans showing the regions from approximately the neck to the knees of the participant with variation due to the subject's height and position in the scanner; (2) Dual energy x-ray absorptiometry (DXA) scans showing the entire body. In total, at the time of data collection, the Biobank consisted of 41,211 DXA scans and 44,830 MR scans from unique participants.

Our collected dataset consists of pairs of same-subject multi-sequence MR and DXA scans, examples of which can be seen in Figure 1. In total we find 20,360 such pairs. These are separated into training, validation and test sets with a 80/10/10% split (16,213, 2,027 and 2,028 scan pairs respectively). Scan pairs are constructed using (1) the fat-only and water-only sequences of the Dixon MR scans, and (2) the tissue and bone images from the DXA scans. For the purposes of this study, we synthesize 2D coronal images from the 3D MR scans by finding the mid-spinal coronal slice at each axial scan line using the method described in [36]. All scans are resampled to be isotropic and cropped to a consistent size for ease of batch processing (501×224 for MR scans and 800×300 for DXA scans). These dimensions maintain an equal pixel spacing of 2.2mm in both modalities. The scans are geometrically related in that the MRI field of view (FoV) is a cropped, translated and slightly rotated transformation of the DXA scan's FoV. Both scans are acquired with the subjects in a supine position, and there can be some arm and leg movements between the scans.

2 Matching Scans Across Modalities

This section describes the framework used to match same-subject scans across the DXA and MRI modalities. As shown in Figure 1, this is hard to perform manually with only a few scans. Differences in tissue types visible in DXA and MRI mean many salient points in one modality are not visible at all in the other. Furthermore, the corresponding scans are not aligned, with variation in subject position, pose and rotation.

To tackle this problem, we use the dual encoder framework shown in Figure 2, tasking it to determine the best alignment between the two scans such that similarity is higher for aligned same-subject scans than for aligned different-subject

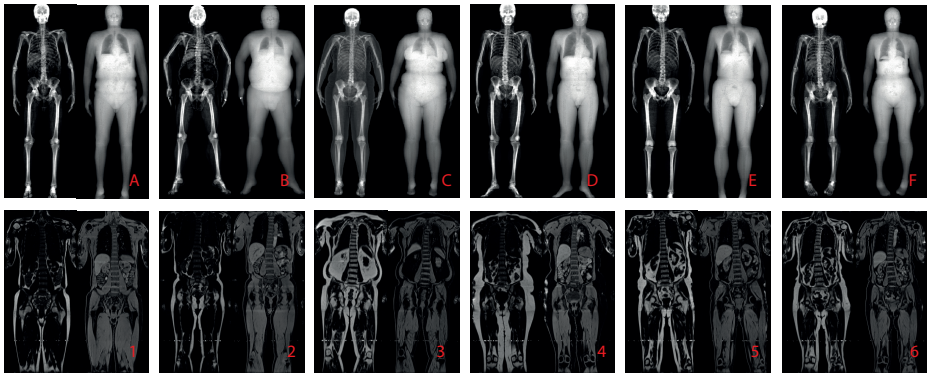


Fig. 1: **Guess Who?** Example scan pairs from our dataset. The top row shows bone (left) and tissue (right) DXA scans from the dataset. The bottom row shows synthesized mid-coronal fat-only (left) and water-only (right) Dixon MR slices. In this paper, semantic spatial representations of the scans are learnt by matching corresponding DXA and MR scan pairs. Can you match these pairs?[1]

scans. Since both the DXA and MRI scans are coronal views and subject rotations relative to the scanner are very small, an approximate alignment requires determining a 2D translation between the scans. The similarity is then determined by a scalar product of the scans' spatial feature maps after alignment. In practice, this amounts to 2D convolution of the MRI's spatial feature map over the DXA's spatial feature map, and the maximum value of the resulting correlation map provides a similarity score.

The network is trained end-to-end by Noise Contrastive Estimation [12] over a batch of N randomly sampled matching pairs. If M_{ij} represents the similarity between the i^{th} DXA and j^{th} MRI, where $i = j$ is a matching pair and $i \neq j$ is non-matching, and τ is some temperature parameter, the total loss for the k-th matching pair, ℓ_k, is given by

$$\ell_k = -\left(\log \frac{\exp(M_{kk}/\tau)}{\sum_{j=1}^{N} \exp(M_{kj}/\tau)} + \log \frac{\exp(M_{kk}/\tau)}{\sum_{j=1}^{N} \exp(M_{jk}/\tau)}\right) \tag{1}$$

2.1 Experiments

This section evaluates the performance of the proposed configuration on the cross-modal scan-matching task. To determine the relative importance of each MRI sequence and each DXA type, we train networks varying input channels to each modality's encoder (see Figure 3 for the configurations used). To demonstrate the value of comparing spatial feature maps of scans instead of a single global embedding vector, we compare to a baseline network that simply pools

[1] $A \to 5$, $B \to 3$, $C \to 4$, $D \to 2$, $E \to 1$, $F \to 6$

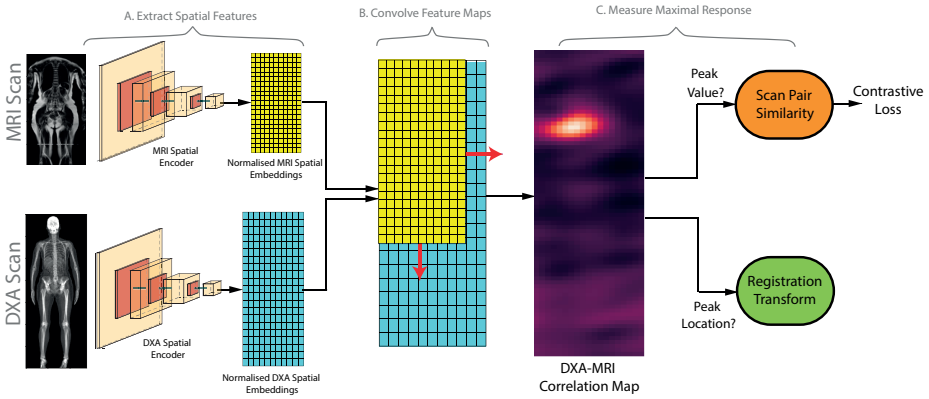


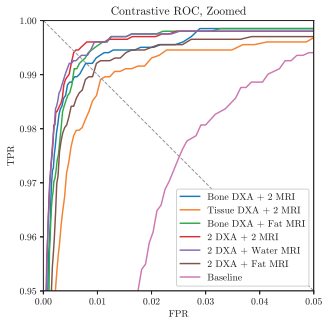
Fig. 2: The dual encoding configuration used for contrastive training. Two CNNs ingest scans of the respective modalities, outputting coarse spatial feature maps (A). The feature maps of each DXA-MRI pair are normalised and correlated to find the best registration (B). Using this registration, the maximum correlation is recorded as the similarity between the two scans (C). The architecture used for both spatial encoders is shown in the appendix.

the spatial feature maps into a scan-level descriptor, and is trained by the same contrastive method. Details of this baseline are given in the appendix.

Implementation. Networks are trained with a batch size of 10 using an Adam optimizer with a learning rate of 10^{-5} and $\beta = (0.9, 0.999)$. A cross-entropy temperature of $T = 0.01$ is used (a study of the effect of varying this is given in the appendix). Spatial embeddings are 128-dimensional. Training augmentation randomly translates the both scans by ± 5 pixels in both axis and alters brightness and contrast by $\pm 20\%$. Each model takes 3 days to train on a 24GB NVIDIA Tesla P40 GPU. Networks are implemented in PyTorch v.1.7.0.

Evaluation measures. We evaluate the quality of the learnt embeddings on the test set by assessing the ability of the system to: (1) retrieve the matching opposite modality scan for a given query scan based on similarity; (2) verify if a given scan pair is matching or not. In the latter case, positive matches to a scan are defined as those with similarities above a threshold, ϕ, and negative matches have similarity $\leq \phi$. Considering all possible DXA-MRI scan pairs (matching & non-matching), we can then generate an ROC curve by varying ϕ from -1 to 1. For the retrieval task, we report top-1 and top-10 recall based on similarity across all test set subjects, and the mean rank of matching pairs. For the verification task, we report the ROC area-under-curve (AUC) and the equal error rate (EER) (i.e. when $TPR = FPR$).

Results. Figure 3 shows the ROC curve and performance measures for varying input channels. All configurations vastly exceed the baseline's performance, indicating the benefit of spatial scan embeddings as opposed to scan-level descriptor



(a) ROC Curve

Input		Verification		Retrieval		
DXA	MRI	AUC	EER (%)	% Recall @1	% Recall @10	Mean Rank
Baseline		0.9952	2.57	26.3	78.7	9.246
B	F	0.9992	0.77	89.4	99.4	2.106
B	F,W	**0.9993**	0.84	87.7	99.4	2.079
T	F,W	0.9986	1.14	83.1	98.4	3.013
B,T	F	0.9989	0.98	85.8	98.7	2.569
B,T	W	**0.9993**	0.70	90.1	99.4	**1.920**
B,T	F,W	0.9992	**0.60**	**90.7**	**99.5**	2.526

(b) Retrieval and Verification Performance

Fig. 3: Verification and retrieval performance on the 2,028 scan test dataset with varying inputs of bone DXA (B), tissue DXA (T), fat-only MR (F), and water-only MR (W). (c) shows an ROC curve for the verification task. Table (b) reports performance statistics for the models, including equal error rate (EER), area under curve (AUC), recall at ranks 1 & 10 and the mean rank of matches.

vectors. The full model achieves a top-1 recall of over 90% from 2028 test cases. The tissue DXA-only model performs worst of all configurations suggesting bone DXAs are much more informative here. Extended results and recall at K curves are given in the appendix.

Discussion. The strong performance of the proposed method on the retrieval task by matching spatial (as opposed to global) features is significant; it suggests the encoders learn useful semantic information about specific regions of both scans. This has several possible applications. For example, one could select a query ROI in a scan, perhaps containing unusual pathology, calculate its spatial embeddings and find similar examples across a large dataset (see [30] for a more detailed discussion of this application). More conventionally, the learnt features could be also used for network initialization in downstream tasks on other smaller datasets of the same modality, potentially increasing performance and data efficiency. As a demonstration of the usefulness of the learnt features, the next section of this paper explores using them to register scans in a completely unsupervised manner.

3 Unsupervised Registration Of Multi-Modal Scans

A major advantage of this contrastive training method is that dense correspondences between multi-modal scans are learnt in a completely self-supervised manner. This is non-trivial; different tissues are shown in each modality, making intensity-based approaches for same- or similar-modality registration [23, 35] ineffective. Here we explore this idea further, developing three methods for estimating rigid registrations between the modalities. Each method is assessed by measuring L2-distance error when transforming anatomical keypoints from the

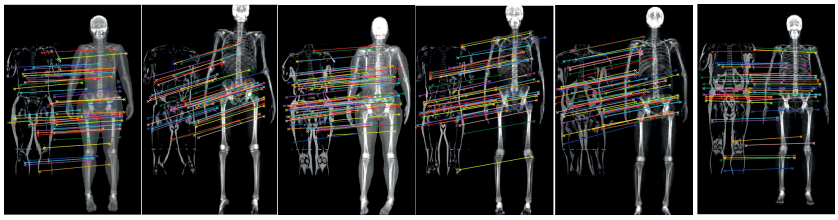


Fig. 4: Salient point correspondences between scan pairs found by Lowe's ratio test & RANSAC. The fat-only channel of MRI source image is shown on the left, with the target DXA bone scan shown on the right

MRIs to the DXA scans. For each proposed registration method the aim is to estimate the three transformation parameters; a 2D translation and a rotation.

1. Dense Correspondences: During training, the contrastive framework attempts to align dense spatial feature maps before comparing them. We can use this to determine the registration translation by convolving the feature maps together and measuring the point of maximum response as the displacement between the images (as in Figure 2, stages A, B). The rotation between the scans is found by rotating the MRI scan across a small range of angles, convolving the feature maps, and recording the angle which induces the greatest alignment.

2. Salient Point Matching: The dense correspondence method is slow, especially on a CPU, as it requires multiple convolution operations with large kernels. To speed up registration we need use only a few salient points between the feature maps. These can be found by matching pairs of points based on correlations and then employing Lowe's second nearest neighbour ratio test [22] to remove ambiguous correspondences, followed by RANSAC estimation of the transformation. Details of this algorithm are given in the appendix. Example correspondences found by this method are shown in Figure 4.

3. Refinement Regressor: The previous approaches generate robust approximate registrations between the two images but are limited by the resolution of the feature maps they compare (8×downsample of a 2.2mm pixel spacing original image). To rectify this issue we use a small regression network to refine predictions by taking the almost-aligned feature maps predicted by the aforementioned methods and then outputting a small refinement transformation. High-precision training data for this task can be generated 'for free' by taking aligned scan pairs from the salient point matching method, slightly misaligning them with a randomly sampled rotation and translation and then training a network to regress this random transformation. The regression network is trained on 50 aligned pairs predicted by the previous salient point matching method and manually checked for accuracy. For each pair, several copies are generated with slight randomly sampled translations and rotations at the original pixel resolution. For each transformed pair, the DXA and MRI spatial feature maps are then concatenated together, and used as input to a small CNN followed by a fully-connected network that estimates the three parameters of the transformation for each pair.

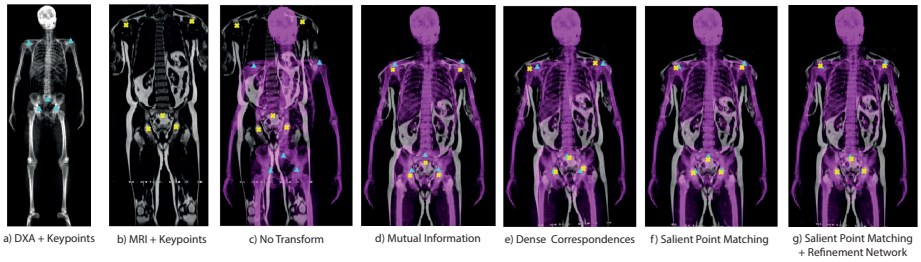


Fig. 5: Example results from each registration method. (a) & (b) show keypoints for the MRI and the DXA. The MRI & keypoints are registered to the DXA by: (c) no transform; (d) mutual information maximisation; (e) Dense correspondences as in pre-training; (f) Salient point matching via Lowe's ratio test; (g) Applying the refinement regressor to (f).

Experiments. To measure the quality of these registrations, 5 keypoints were marked in 100 test scan pairs: the femoral head in both legs (hip joints), humerus head in both arms (shoulder joints) and the S1 vertebra (base of the spine). MRI keypoints are annotated in 3D and then projected into 2D. These keypoints provide the ground truth for assessing the predicted transformations. Example annotations are shown in Figure 5. We then measure the mean L2-localisation error when transferring the keypoints between modalities using rigid body transforms predicted by the proposed methods. We compare to baselines of (i) no transformation (i.e. the identity); and (ii) rigid mutual information maximisation[2]. To measure annotation consistency and error induced by change in subject pose, we also report the error of the 'best-possible' rigid transformation keypoints - that which minimises the mean L2 transfer error.

Results. Table 1 shows the localisation error achieved by each method. All methods yield accurate registrations between the images. The best method is found to salient point matching followed by the refinement network, which is also shown to be fast on both a GPU and CPU. We attempted to calculate SIFT and MIND features in both modalities and match them as proposed in [34] and [15] repectively however these approaches did not work in this case (see appendix).

Discussion. In this setting, our methods were found to outperform other approaches for multi-modal registration (mutual information, MIND and SIFT). We believe the reason for this is that DXA scans show mostly bony structures, whereas most visual content in MRI is due to soft tissues which can't be differentiated by DXA. As such, most pixels have no obvious intensity relation between scans. However, accurate registration between the scans is important as it allows collation of spatial information from both modalities. This can be exploited in at least two ways: (i) for joint features; registration allows shallow fusion of spatial features from both modalities. This could be useful in, for example, body composition analysis, conventionally done by DXA but which may benefit from the superior soft tissue contrast of MRI [5]. (ii) for cross-modal supervision; registra-

[2] Using MATLAB's `imregister` with `MattesMutualInformation` [24] as an objective.

tion allows prediction of dense labels from one modality which can then be used as a training target for the other. For example one could diagnose osteoporosis/ fracture risk at a given vertebral level from MR using labels extracted from DXA by conventional methods.

Method	Keypoint Transfer Error (cm)					Time(s)	
	HJ	S1	SJ	Median(all)	Mean(all)	GPU	CPU
No Trans.	22.1±5.0	21.7±5.3	22.3±5.0	21.9	22.01±5.1	0	0
Mut. Inf.	2.23±1.3	2.67±1.4	2.75±2.2	2.21	2.52±1.7	-	1.0
Dense Corr.	1.48±0.8	1.52±0.8	2.05±1.2	1.52	1.72±1.0	1.5	5.7
Sal. Pt. Mt.	1.34±0.9	1.37±1.0	2.04±1.4	1.46	1.63±1.3	0.4	1.1
Regressor	1.24±0.8	1.30±0.9	1.44±0.9	1.12	1.32±0.9	0.9	1.5
Best Poss.	0.84±0.4	0.84±0.5	0.87±0.4	0.84	0.87±0.4	-	-

Table 1: Keypoint transfer error for the proposed methods. We report the mean and median error for all keypoints combined and for the hip joints (HJ), shoulder joints (SJ) and S1 individually. Runtime on a GPU & CPU is also shown.

3.1 Cross-Modal Annotation Transfer

A benefit of the demonstrated cross-modal registrations is that they allow the transfer of segmentations between significantly different modalities, meaning segmentation networks can be trained in both modalities from a single annotation set. This is useful in cases when a tissue is clearly visible in one modality but not the other. For example, here the pelvis is clearly visible in the DXA scan but not in the MRI slice. As an example of using cross-modal annotation transfer, the spine, pelvis and pelvic cavity are segmentated in DXA scans using the method from [18]. These segmentations are then transferred to the MRI scans by the refinement network from section 3. where they act as pixel-wise annotations to train a 2D U-Net [29] segmentation network. Compared to manual segmentation of the spine performed in 50 3D MR scans and projected into 2D, this network achieves good performance, with a mean Dice score of 0.927 showing the quality of the transferred annotations. Examples are shown in the appendix.

4 Conclusion

This paper explores a new self-supervised task of matching different-modality, same-subject whole-body scans. Our method to achieves this by jointly aligning and comparing scan spatial embeddings via noise contrastive estimation. On a test dataset of 2028 scan pairs our method is shown to perform exceptionally well with over 90% top-1 recall. We then show the learnt spatial embeddings can be used for unsupervised multi-modal registration in cases where standard

approaches fail. These registrations can then be used to perform cross-modal annotation transfer, using DXA segmentations to train a MRI-specific model to segment anatomical structures. Future work will explore using the learnt spatial embeddings for other downstream tasks and extend this method to 3D scans.

Acknowledgements. Rhydian Windsor is supported by Cancer Research UK as part of the EPSRC CDT in Autonomous Intelligent Machines and Systems (EP/L015897/1). We are also grateful for support from a Royal Society Research Professorship and EPSRC Programme Grant Visual AI (EP/T028572/1).

References

1. Alwassel, H., Mahajan, D., Korbar, B., Torresani, L., Ghanem, B., Tran, D.: Self-Supervised Learning by Cross-Modal Audio-Video Clustering. In: NeurIPS (2020)
2. Arandjelović, R., Zisserman, A.: Look, listen and learn. In: Proc. ICCV (2017)
3. Arandjelović, R., Zisserman, A.: Objects that sound. In: Proc. ECCV (2018)
4. Asano, Y.M., Rupprecht, C., Vedaldi, A.: Self-labelling via simultaneous clustering and representation learning. In: Proc. ICLR (2020)
5. Borga, M.: MRI adipose tissue and muscle composition analysis—a review of automation techniques. The British Journal of Radiology **91**(1089), 20180252 (2018)
6. Brown, T., et al.: Language models are few-shot learners. In: NeurIPS (2020)
7. Caron, M., Misra, I., Mairal, J., Goyal, P., Bojanowski, P., Joulin, A.: Unsupervised learning of visual features by contrasting cluster assignments. In: NeurIPS (2020)
8. Chen, Ting and Kornblith, Simon and Norouzi, Mohammad and Hinton, Geoffrey: A Simple Framework for Contrastive Learning of Visual Representations. In: Proc. ICLR (2020)
9. Devlin, J., Chang, M.W., Lee, K., Toutanova, K.: BERT: Pre-training of Deep Bidirectional Transformers for Language Understanding. In: Proc. NAACL. p. 4171–4186 (2019)
10. Ghorbani, A., Natarajan, V., Coz, D., Liu, Y.: Dermgan: Synthetic generation of clinical skin images with pathology. In: Machine Learning for Health NeurIPS Workshop. pp. 155–170 (2019)
11. Grill, J.B., Strub, F., Altché, F., Tallec, C., Richemond, P., Buchatskaya, E., Doersch, C., Avila Pires, B., Guo, Z., Gheshlaghi Azar, M., Piot, B., Kavukcuoglu, K., Munos, R., Valko, M.: Bootstrap your own latent - a new approach to self-supervised learning. In: NeurIPS (2020)
12. Gutmann, M.U., Hyvärinen, A.: Noise-contrastive estimation of unnormalized statistical models, with applications to natural image statistics. Journal of Machine Learning Research **13**(11), 307–361 (2012)
13. Han, T., Xie, W., Zisserman, A.: Self-supervised co-training for video representation learning. In: NeurIPS (2020)
14. He, K., Fan, H., Wu, Y., Xie, S., Girshick, R.: Momentum contrast for unsupervised visual representation learning. In: Proc. CVPR (2020)
15. Heinrich, M.P., Jenkinson, M., Bhushan, M., Matin, T., Gleeson, F.V., Brady, S.M., Schnabel, J.A.: MIND: Modality independent neighbourhood descriptor for multi-modal deformable registration. In: Proc. MICCAI (2012)
16. Hénaff, O., Srinivas, A., De Fauw, J., Razavi, A., Doersch, C., Ali Eslami, S., van den Oord, A.: Data-efficient image recognition with contrastive predictive coding. In: Proc. ICLR (2020)

17. Howard, Jeremy and Ruder, Sebastian: Universal Language Model Fine-tuning for Text Classification. In: Proc. ACL (2018)
18. Jamaludin, A., Kadir, T., Clark, E., Zisserman, A.: Predicting scoliosis in dxa scans using intermediate representations. In: MICCAI Workshop: Computational Methods and Clinical Applications for Spine Imaging (2018)
19. Jamaludin, A., Kadir, T., Zisserman, A.: Self-Supervised Learning for Spinal MRIs. In: MICCAI Workshop on Deep Learning in Medical Image Analysis (2017)
20. Johnson, A.E.W., et al.: MIMIC-CXR, a de-identified publicly available database of chest radiographs with free-text reports. Scientific Data **6**(1), 317 (2019)
21. Korbar, B., Tran, D., Torresani, L.: Cooperative learning of audio and video models from self-supervised synchronization. In: NeurIPS. vol. 31 (2018)
22. Lowe, D.: Object recognition from local scale-invariant features. In: Proc. ICCV. pp. 1150–1157 (Sep 1999)
23. Lowe, D.: Distinctive image features from scale-invariant keypoints. IJCV **60**(2), 91–110 (2004)
24. Mattes, D., Haynor, D.R., Vesselle, H., Lewellyn, T.K., Eubank, W.: Nonrigid multimodality image registration. In: Sonka, M., Hanson, K.M. (eds.) Medical Imaging 2001: Image Processing. vol. 4322, pp. 1609 – 1620. International Society for Optics and Photonics, SPIE (2001), https://doi.org/10.1117/12.431046
25. Mikolov, T., Sutskever, I., Chen, K., Corrado, G.S., Dean, J.: Distributed representations of words and phrases and their compositionality. In: NeurIPS (2013)
26. Owens, A., Efros, A.A.: Audio-visual scene analysis with self-supervised multisensory features. In: Proc. ECCV (2018)
27. Qian, R., Meng, T., Gong, B., Yang, M.H., Wang, H., Belongie, S., Cui, Y.: Spatiotemporal contrastive video representation learning. In: Proc. CVPR (2021)
28. Radford, A., Wu, J., Child, R., Luan, D., Amodei, D., Sutskever, I.: Language models are unsupervised multitask learners. Tech. rep., OpenAI (2019)
29. Ronneberger, O., Fischer, P., Brox, T.: U-net: Convolutional networks for biomedical image segmentation. In: Proc. MICCAI. pp. 234–241 (2015)
30. Simonyan, K., Zisserman, A., Criminisi, A.: Immediate structured visual search for medical images. In: Proc. MICCAI (2011)
31. Sudlow, C., Gallacher, J., Allen, N., Beral, V., Burton, P., Danesh, J., Downey, P., Elliott, P., Green, J., Landray, M., Liu, B., Matthews, P., Ong, G., Pell, J., Silman, A., Young, A., Sprosen, T., Peakman, T., Collins, R.: Uk biobank: An open access resource for identifying the causes of a wide range of complex diseases of middle and old age. PLOS Medicine **12**(3), 1–10 (2015)
32. Taleb, A., Lippert, C., Klein, T., Nabi, M.: Multimodal self-supervised learning for medical image analysis. In: Proc. IPMI (2021)
33. Taleb, A., Loetzsch, W., Danz, N., Severin, J., Gaertner, T., Bergner, B., Lippert, C.: 3d self-supervised methods for medical imaging. In: NeurIPS (2020)
34. Toews, M., Zöllei, L., Wells, W.M.: Feature-based alignment of volumetric multimodal images. In: Gee, J.C., Joshi, S., Pohl, K.M., Wells, W.M., Zöllei, L. (eds.) Information Processing in Medical Imaging. pp. 25–36. Springer Berlin Heidelberg (2013)
35. Viola, P., Wells, W.: Alignment by maximization of mutual information. In: Press, I.C.S. (ed.) Proc. ICCV. pp. 16–23 (Jun 1995)
36. Windsor, R., Jamaludin, A., Kadir, T., Zisserman, A.: A convolutional approach to vertebrae detection and labelling in whole spine MRI. In: Proc. MICCAI (2020)

5 Appendix

5.1 Scan Matching - Architecture, Extended Tables & Figures

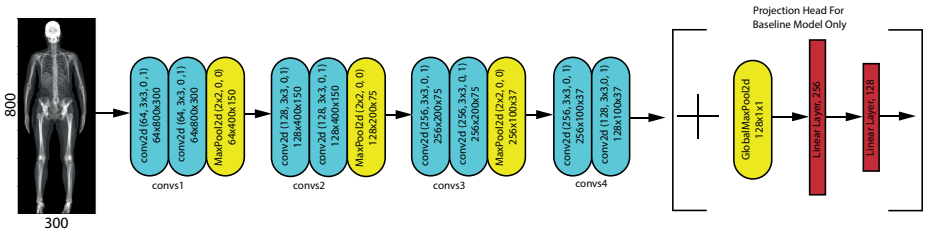
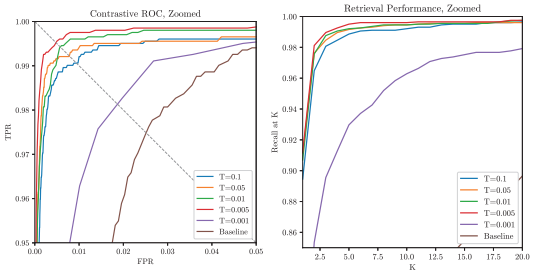
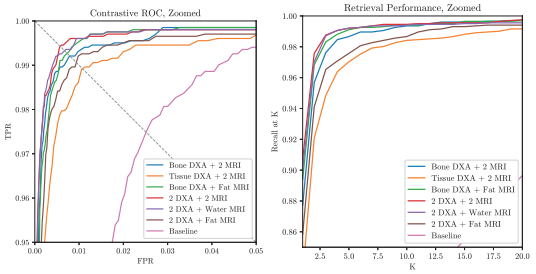


Fig. 6: The simple spatial encoder used in the contrastive framework. Both the MR and DXA spatial encoders use this architecture. For the baseline model, the output spatial features are max pooled and the projection head shown on the right is appended. Each convolutional & linear layer except the final one uses ReLU activations, followed by BatchNorm.



(a) Temperature ROC

(b) Temperature R@K



(c) Input-varying ROC

(d) Input-varying R@K

Fig. 7: ROC and Recall at K (R@K) curves for varying scan-input and temperature parameter τ.

Input Scans	% Recall			AUC	Mean Rank	Equal Error Rate	TPR@ FPR=1%
	Top-1	Top-5	Top-10				
Bone DXA + Fat MRI	89.41	99.11	99.41	0.9992	2.106	0.0077	0.9955
Bone DXA + 2 MRI	87.72	98.66	99.36	**0.9993**	2.079	0.0084	0.9935
Tissue DXA + 2 MRI	83.12	97.03	98.42	0.9986	3.013	0.0114	0.9891
2 DXA + Fat MRI	85.84	97.57	98.66	0.9989	2.569	0.0098	0.9925
2 DXA + Water MRI	90.05	**99.21**	99.41	0.9993	**1.920**	0.0070	**0.9960**
2 DXA + 2 MRI	**90.69**	**99.21**	**99.46**	0.9992	2.526	**0.0060**	**0.9960**

Table 2: An extended table of performance metrics for varying scan-input in contrastive training including true positive rate at a false positive rate of 1% (TPR@FPR=1%) and top-5 recall.

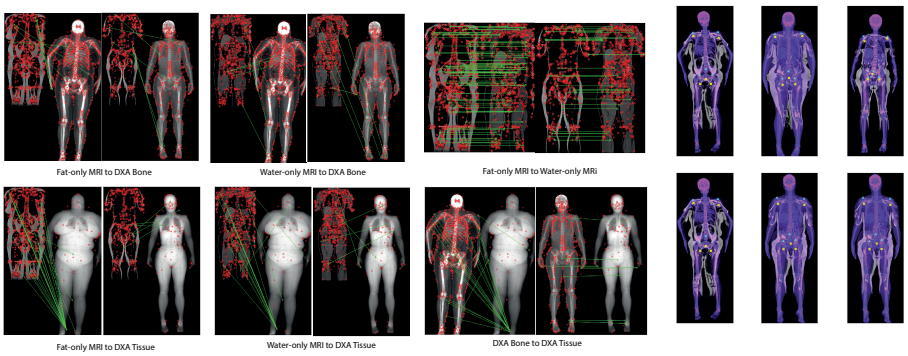
Temperature, τ	% Recall			AUC	Mean Rank	Equal Error Rate	TPR@ FPR=1%
	Top-1	Top-5	Top-10				
τ=0.1	89.46	98.86	99.41	0.9991	2.148	0.0095	0.9921
τ=0.05	91.14	99.16	99.45	0.9991	**2.140**	0.0080	0.9946
τ=0.01	90.07	99.21	99.45	0.9992	2.527	0.0060	0.9960
τ=0.005	**91.18**	**99.50**	**99.60**	**0.9994**	2.214	**0.0049**	**0.9975**
τ=0.001	74.41	92.97	96.28	0.9979	3.534	0.0197	**0.9629**

Table 3: Scan-matching performance metrics for configurations with varying softmax temperature, τ.

5.2 Unsupervised Registration

Lowe's Nearest Neighbours Ratio Test

1. For pixel in source feature map s_1, find the top-two most correlating pixels in the target feature map, t_1 and t_2 respectively.
2. If $\tau \cdot sim(s_1, t_1) < sim(s_1, t_2)$ save the pair (s_1, t_1), where τ is some threshold between 0 and 1 and sim is the cosine similarity.
3. Repeat this for each pixel in the source feature map to obtain a set of candidate matches between the feature maps.
4. Apply RANSAC to remove spurious correlations from these candidates
5. Use LMEDS to get the best rigid transform between remaining inlying points.



(a) SIFT Correspondences

(b) Non-rigid MIND Registration

Fig. 8: **Attempted registration using SIFT & MIND features for the varying modalities**. a) SIFT features (shown by red circles) were calculated in both the original image and a negative version. They are then matched across modalities by brute-force matching and RANSAC is applied to find the best affine transform between the images. The in-lying matches are shown in green. This approach only succeeds finding correspondances between the already aligned MR sequences and to, some extent, the DXA images. b) Results from Gauss-Newton optimised non-rigid MIND registration results as implemented at `https://github.com/cmirfin/BBR`.

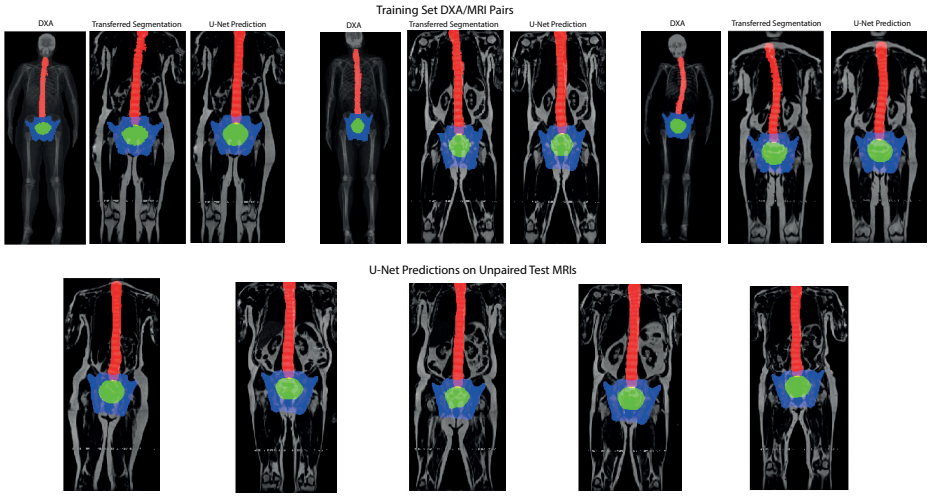


Fig. 9: **Predicted segmentations of the spine, pelvis and pelvic cavity in MR scans by a U-Net trained with DXA annotations**. Structures are segmented in DXA scans and transferred to the corresponding MR scan by the refinement registration method. A model is trained on the transferred segmentations which can then be applied to unpaired MR scans.